Synthetic and Systems Biotechnology 8 (2023) 640–646

Contents lists available at ScienceDirect

Synthetic and Systems Biotechnology

journal homepage: www.keaipublishing.com/en/journals/synthetic-and-systems-biotechnology

Nobachelins, new siderophores from *Nocardiopsis baichengensis* protecting *Caenorhabditis elegans* from *Pseudomonas aeruginosa* infection

Haowen Zhao [a,b,c,1], Yuhao Ren [a,d,1], Feng Xie [a], Huanqin Dai [e], Hongwei Liu [e], Chengzhang Fu [a,b], Rolf Müller [a,b,*]

[a] Helmholtz Institute for Pharmaceutical Research Saarland (HIPS), Helmholtz Centre for Infection Research (HZI), and Department of Pharmacy, Saarland University, 66123, Saarbrücken, Germany
[b] Helmholtz International Lab for Anti-Infectives, Helmholtz Center for Infection Research, 38124, Braunschweig, Germany
[c] Institute of Marine Biology and Pharmacology, Ocean College, Zhejiang University, 316021, Zhoushan, China
[d] State Key Laboratory of Drug Research, Shanghai Institute of Materia Medica, Chinese Academy of Sciences, 555 Zuchongzhi Road, 201203, Shanghai, China
[e] State Key Lab of Mycology, Institute of Microbiology, Chinese Academy of Sciences, 100101, Beijing, China

ARTICLE INFO

Keywords:
Nocardiopsis
Genome mining
Siderophore
Pseudomonas aeruginosa
Infection

ABSTRACT

The biosynthetic potential of actinobacteria to produce novel natural products is still regarded as immense. In this paper, we correlated a cryptic biosynthetic gene cluster to chemical molecules by genome mining and chemical analyses, leading to the discovery of a new group of catecholate-hydroxamate siderophores, nobachelins, from *Nocardiopsis baichengensis* DSM 44845. Nobachelin biosynthesis genes are conserved in several bacteria from the family *Nocardiopsidaceae*. Structurally, nobachelins feature fatty-acylated hydroxy-ornithine and a rare chlorinated catecholate group. Intriguingly, nobachelins rescued *Caenorhabditis elegans* from *Pseudomonas aeruginosa*-mediated killing.

1. Introduction

The rapid accumulation of genome sequence information has revealed the vast microbial biosynthetic potential and metabolic diversity that has yet to be fully explored, where actinobacteria are especially rich in structurally diverse and biologically active natural products [1]. However, the traditional methods of natural product discovery from actinobacteria are time-consuming and labor-intensive and often result in the rediscovery of known compounds [2]. Therefore, more efficient approaches are needed. One strategy is to combine bioinformatics and mass spectrometry to rapidly identify and characterize novel natural products from genomic and metabolomic data [3,4]. Automated bioinformatics platforms can compare biosynthetic gene clusters (BGCs) in genomic sequence data to those of previously sequenced microorganisms [5]. This enables the rapid estimation of the biosynthetic potential for natural products and the inference of their structures from biosynthetic principles. The mass spectrometry-based techniques can detect and analyze the metabolites produced by actinobacteria under different conditions and match them with the predicted structures [4,6,7]. This integrated approach can significantly accelerate the discovery and characterization of novel natural products.

Siderophores are an important class of natural products with a high affinity for binding and solubilizing ferric iron (Fe^{3+}), essential for many bacterial species' growth, survival, and pathogenesis [8]. Siderophores offer promising opportunities for medical applications [9], such as the treatment of iron overload [10], delivery of antibiotics in infection therapy [11], molecular imaging of infection [12], and as inhibitors of metalloenzymes for the treatment of cancer [13]. Moreover, siderophores have recently been shown to inhibit the *Pseudomonas aeruginosa*-mediated killing of *Caenorhabditis elegans*, even though they have no direct bactericidal activity [14]. This finding highlights the exciting potential of siderophores in anti-infection research by modulating host-pathogen interactions. Therefore, the nonbactericidal siderophores could be an attractive target for discovering anti-infectives with novel mode-of-action that may help to prevent the rapid emergence of resistance frequently observed with bactericidal antibiotics. Siderophores

Peer review under responsibility of KeAi Communications Co., Ltd.
* Corresponding author. Helmholtz Institute for Pharmaceutical Research Saarland (HIPS), Helmholtz Centre for Infection Research (HZI), and Department of Pharmacy, Saarland University, 66123, Saarbrücken, Germany.
E-mail address: rolf.mueller@helmholtz-hips.de (R. Müller).
[1] These authors contributed equally to this work.

https://doi.org/10.1016/j.synbio.2023.09.007
Received 14 June 2023; Received in revised form 17 September 2023; Accepted 21 September 2023
Available online 29 September 2023

are generally classified according to the functional group for the metal binding, including catecholate, phenolate, hydroxamate, and carboxylate compounds [15]. However, siderophores are also often found to contain different functional groups in the same molecule [16]. Siderophore biosynthetic pathways are diverse, mainly distinguished as nonribosomal peptide synthetases (NRPSs) or NRPS-independent enzymes [17], making them readily identifiable by bioinformatic prediction. Moreover, recent genome mining efforts have shown that siderophore BGCs are widely distributed in *Actinobacteria* [14,18].

So far, many siderophores have been identified from various bacterial species [19]. To find uncharacterized siderophores with potential bioactivity, we focused on rare *Actinobacteria* in the absence of previous reports of siderophores, such as strains from the genus *Nocardiopsis*, which has been recognized to be a prolific source of bioactive natural products [20–22]. The *in-silico* genome mining highlighted one putative siderophore BGC from the strain *Nocardiopsis baichengensis* DSM 44845. Herein, we report the isolation, structure elucidation, biosynthesis proposal, and anti-infection bioactivity of nobachelins A-C (**1**–**3**), a new hybrid-type catecholate-hydroxamate siderophore containing fatty acyl-modified hydroxy-ornithine and a rare 4-chloro-2,3-dihydroxy--benzoic acid (CDB).

2. Materials and methods

2.1. General experimental procedures

One-dimensional (1D) and two-dimensional (2D) nuclear magnetic resonance (NMR) spectra were recorded on a 500 MHz (megahertz) Avance III (UltraShield) spectrometer or a 700 MHz Avance III (Ascend) spectrometer, each equipped with a Helium-cooled CryoProbe (TCI). All observed chemical shift values (δ) are given in ppm (parts per million) and coupling constant values (J) in Hz. The spectra were recorded in DMSO-d_6 (dimethyl sulfoxide-d_6), and chemical shifts of the solvent signal at δ_H 2.50 ppm and δ_C 39.5 ppm were used as reference signals for spectra calibration. High-resolution electrospray ionization mass spectroscopy (HRESIMS) spectra were measured on a maXis4G high resolution TOF (time of flight) mass spectrometer (Bruker Daltonics) coupled with a Dionex high-performance liquid chromatography (HPLC) (Thermo Scientific).

2.2. Fermentation and isolation of compounds 1–3

The strain *N. baichengensis* DSM 44845 was obtained from the DSMZ strain collection (Braunschweig, Germany) and its genome sequence was retrieved from GenBank (GCA_000341205.1). The strain was maintained on the ISP4 agar plate (10 g/L soluble starch, 1 g/L dipotassium phosphate, 1 g/L magnesium sulfate, 1 g/L sodium chloride, 2 g/L ammonium sulfate, 2 g/L calcium carbonate, 1 mg/L ferrous sulfate, 1 mg/L manganous chloride, 1 mg/L zinc sulfate, 20 g/L agar). For fermentation, fresh spores were collected from the agar plate and inoculated into TSB medium (17 g/L tryptone, 3 g/L soytone, 2.5 g/L glucose, 5 g/L sodium chloride, 2.5 g/L dipotassium hydrogen phosphate) and incubated at 30 °C with shaking. The resulting seed culture was used to inoculate fresh M1 medium (10 g/L glucose, 7 g/L peptone, 3 g/L meat extract, 3 g/L sodium chloride and 2 g/L dipotassium hydrogen phosphate, pH 7.0). The fermentation was continued for 8 days at 30 °C while shaking at 120 rpm.

To the fermentation culture (2L), XAD-16 resin was added and shaken for 2 h. The XAD-16 resin was extracted with acetone three times, and solvents were then combined and dried under reduced pressure to give the crude extract. The resulting crude extract was first dispersed in water and then partitioned using ethyl acetate three times. The organic phase was combined and dried in *vacuum* and subsequently fractioned using Sephadex LH20 column (GE Healthcare), with methanol as the mobile phase. Fractions were collected and pooled based on the LC-MS analysis. Further purification was performed using a Dionex Ultimate 3000 low pressure gradient system equipped with a Waters XSelect Peptide CSH C18 column (5 μm, 10 × 250 mm). Purification was carried out under the following HPLC conditions: solvent A, Milli-Q water (0.1% formic acid); solvent B, acetonitrile (0.1% formic acid); at 45 °C with a flow rate of 5 mL/min. The gradient was 35% B to 50% B in 20min. **1** was eluted at 11.08 min (3 mg), **2** was eluted at 14.60 min (9 mg), and **3** was eluted at 18.19 min (4 mg).

2.3. Marfey's method

Compound **2** was hydrolyzed in 6 N HCl (200 μL) at 110 °C for 1 h and then dried under nitrogen flow. The obtained hydrolysate was dissolved in H_2O (110 μL), and the solution was split into two (50 μL each). To each aliquot, 20 μL 1 N $NaHCO_3$ and 20 μL 1% Marfey's reagent (one L-FDLA and the other D-FDLA) were added. The reaction mixture was incubated at 45 °C, 700 rpm for 2 h. The reaction solutions were neutralized with 2 N HCl (10 μL) and diluted with 300 μL acetonitrile. Standards were derivatized in the same fashion. Derivatives were centrifuged and analyzed by LC-MS. The condition used was as follows: ACQUITY BEH column (100 × 2.1 mm, 1.7 μm, 130 Å); flowrate at 0.6 mL/min and column temperature at 45 °C; H_2O (0.1% formic acid) as eluent A and acetonitrile (0.1% formic acid) as eluent B. 0–1 min: linear increase of eluent B from 5% to 10%; 1–15 min: linear increase of eluent B to 35%; 15–22 min: linear increase of eluent B to 55%; 15–22 min: linear increase of eluent B to 80%; The MS detection was performed in positive mode. Retention times of FDLA-derivatized amino acids are listed in Table S4.

2.4. P. aeruginosa-C. elegans pathogenesis assay

The *P. aeruginosa-C. elegans* liquid killing assay was performed as previously described [23–25]. Briefly, the *sek-1* (*km4*) mutant animals at the late L4 larval stage were infected by *P. aeruginosa* PA14 and then incubated on agar plate. Tested compounds were added into the medium when preparing agar plates. Allow the worms to recover for a few hours, and then start the first time point, score the worms as dead or alive at different times. Survival rate = (Number of alive worms/Total worms) × 100. Assays were performed in quadruplicate; each biological replicate contained 20 worms.

3. Results and discussion

3.1. Identification of a catechol-peptide siderophore gene cluster

In-silico analysis of the genome of *N. baichengensis* DSM 44845 by antiSMASH identified one nonribosomal peptide synthetase (NRPS) gene cluster (*nch*) (Fig. S1, Table S1) [5]. *Nch* is mainly comprised of two NRPS encoding genes (*nchG* and *nchH*), a predicted 2,3-dihydroxybenzoate (2,3-DHB) recognizing stand-alone adenylation (A) domain encoding gene (*nchC*), a discrete peptidyl carrier protein (PCP) gene (*nchF*), as well as a 2,3-DHB formation cassette (*nchABD*), in line with the general feature of aryl-capped type siderophore gene cluster [14,26]. We also found a lysine/ornithine *N*-monooxygenase (NchE) and a GCN5-related *N*-acetyltransferase (NchJ) encoding genes in *nch* that show homology to reported siderophore biosynthesis enzymes [27,28]. Combining the *in-silico* analysis, the backbone sequence of the product was predicted to be (2,3-DHB)-(Gly)-(Gly)-(-Ser)-(Ser)-(δ-*N*-acyl-δ-*N*-hydroxy-ornithine (haOrn))/(δ-*N*-hydroxy-ornithine (hOrn))-(hOrn). However, no clear consensus prediction could be made about the substrate specificity of the first A domain in NchH (Fig. S1, Table S2). The predicted structure was used to query the CAS database (American Chemical Society). No hits with the same peptide sequence were found, suggesting the *nch* cluster might produce new siderophores.

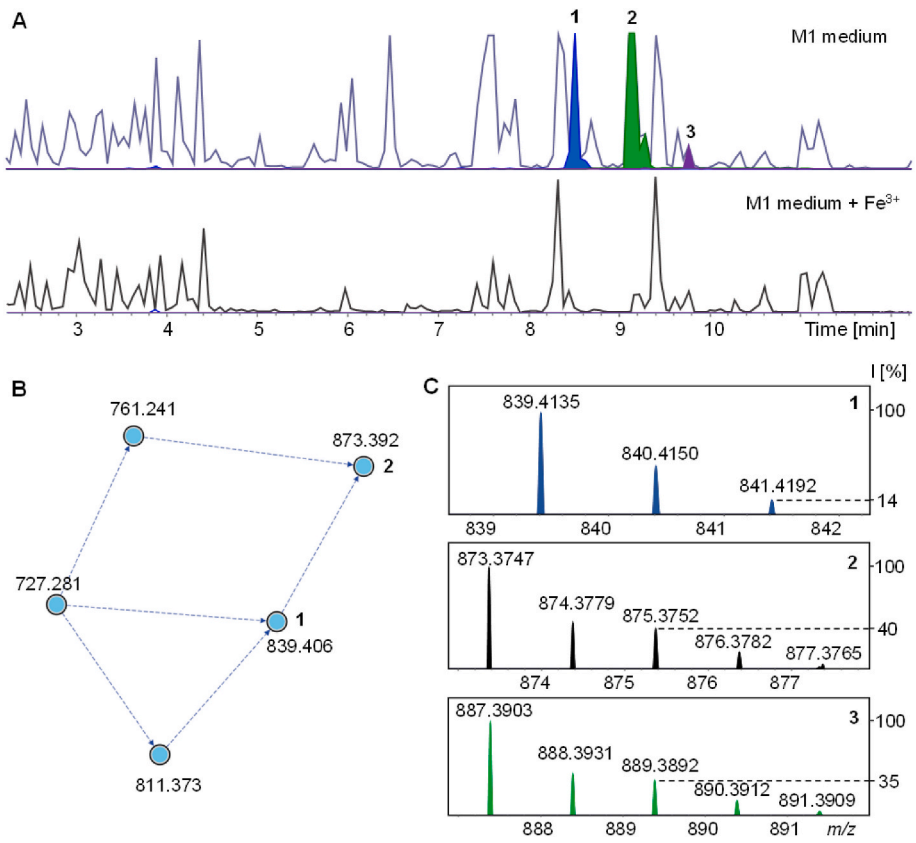

Fig. 1. LC-MS analysis of the culture extract of *N. baichengensis* DSM 44845. (A) Base peak chromatogram from LC-MS analysis of culture extracts in M1 medium or ferric-supplemented M1 medium. (B) Selected molecular network generated from GNPS. (C) HRMS chromatogram of nobachelins A-C (**1**–**3**). **2**–**3** showed characteristic isotope patterns indicating the presence of chlorine.

3.2. HRMS analysis reveals the production of nobachelins

To access the putative siderophores, we cultured *N. baichengensis* using the previously developed strategy [14], specifically by examining variations between media with and without the addition of iron. As expected, a panel of peaks observed in medium M1 was not found when supplemented with 100 μM $FeCl_3$ (Fig. 1A) and were thus assumed to be the targeted siderophores. We applied Global Natural Product Social Molecular Networking (GNPS) [7] to the mass spectrometry data and found that the potential targets clustered together (Fig. 1B). The two most prominent mass peaks (**1**, **2**) with *m/z* 839.406 $[M + H]^+$ and 873.392 $[M + H]^+$ were further analyzed. The MS/MS data of **1** showed a distinct and evident fragmentation pattern (*b*2-*b*5 and *y*2-*y*5) consistent with a DHB-Gly-Gly-Ser-Ser peptide sequence (Fig. 2, Fig. S6). A major MS/MS fragment ion (*b*5) with *m/z* 425.1306 $[M + H]^+$ (calcd. 425.1306) resulting from the loss of two C-terminal residues was observed, which could be associated with the pentapeptide ion of DHB-Gly-Gly-Ser-Ser. In addition, fragment ions corresponding to the sequential loss of two Ser residues and one Gly residue were readily detected (*b*2-*b*4), strongly indicating that **1** is the targeted compound. On the other hand, **2** exhibited a fragmentation pattern that was highly similar to that of **1**. The major difference was the mass shift of +34 Da for the *b* ions (Fig. S6). Moreover, the HRMS spectrum of **2** showed a characteristic isotope pattern, with two peaks separated by 2 *m/z* units showing an intensity ratio of 3:1, indicating the presence of one chlorine atom (Fig. 1C). Furthermore, manual inspection revealed a mass peak (**3**) with *m/z* 887.3902 $[M + H]^+$, which showed a fragmentation pattern that closely resembled that of **2** (Fig. S6).

3.3. Structure elucidation of nobachelins

Next, we sought to purify these compounds from scaled-up fermentation to confirm their structures. After several rounds of purification, sufficient amounts of nobachelins were obtained for structure elucidation by extensive NMR experiments, chemical degradation and derivatization.

Nobachelin A (**1**) has a molecular formula of $C_{37}H_{58}N_8O_{14}$ deduced based on the ion mass at *m/z* 839.4141 $[M + H]^+$ (calcd. for 839.4135), implying thirteen degrees of unsaturation. Careful interpretation of the 1D and 2D NMR spectra revealed that **1** contains two glycine, two serine and two ornithine residues, and one 2,3-dihydroxybenzoate unit. In addition, one unexpected fatty acyl group, 8-methylnonanoate, was revealed by analysis of the NMR data (see Table 1). This acyl group was found attached to the δ-*N* of one ornithine residue, as evidenced by the HMBC (heteronuclear multiple bond correlation) correlations from H-5 (δ_H 3.50, δ_H 3.40, haOrn5) and H-2′ (δ_H 2.32, haOrn5) to C-1′ (δ_C 173.0, haOrn5). On the other hand, the other ornithine was assigned as cyclo-δ-*N*-hydroxy-ornithine (chOrn6) based on the HMBC correlation from H-5 (δ_H 3.45, chOrn6) to C-1 (δ_C 164.7, chOrn6). Furthermore, **1** contained eight peptide bonds while only six α-amide protons were observed, together with the MS/MS data, indicating the δ-*N*-hydroxylation of the two ornithine residues. The presence of two hydroxamate groups was further corroborated by the ^1H–^{15}N HMBC correlations observed for **2** (Table S3). Finally, the connectivity of 2,3-DHB and six amino acid residues was unambiguously determined according to the HMBC correlations in accordance with the MS/MS data.

Nobachelin B (**2**) and C (**3**) were assigned a molecular formula of $C_{37}H_{57}ClN_8O_{14}$ and $C_{38}H_{59}ClN_8O_{14}$, respectively. The occurrence of chlorine in **2** and **3** was recognizable by the characteristic isotope pattern (Fig. 1). The ^1H and ^{13}C NMR spectra of **2** were almost identical

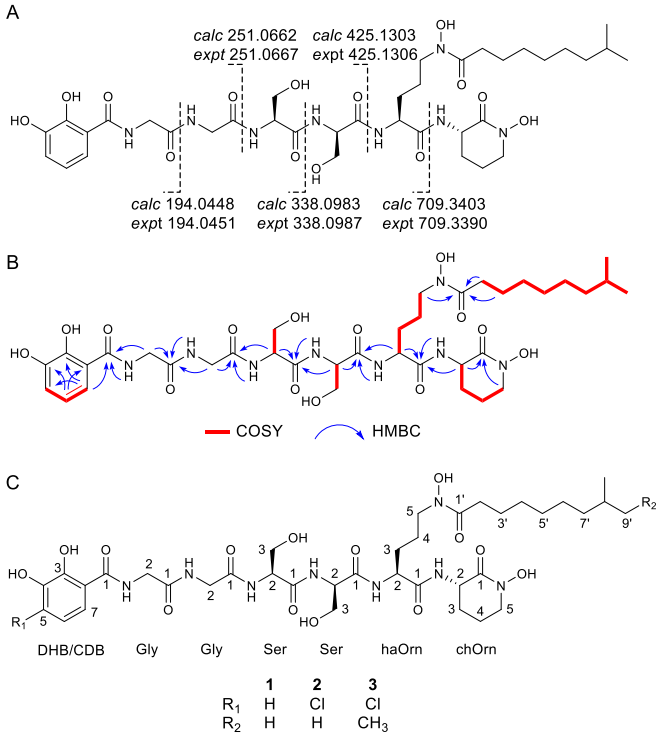

Fig. 2. Structure of nobachelins. (A) MS/MS fragmentation data observed for **1**. (B) Key NMR correlations for **1** (COSY correlations in red and HMBC correlations as blue arrows). (C) Chemical structures of **1**–**3**. Abbreviations of moieties are shown: dihydroxybenzoate (DHB), 4-chloro-dihydroxybenzoate (CDB), glycine (Gly), serine (Ser), δ-*N*-acyl-δ-*N*-hydroxy-ornithine (haOrn), cyclo-δ-*N*-hydroxy-ornithine (chOrn).

to that of **1**, except for the H-5 (δ_H 6.92, 2,3-DHB) in **1** which was absent in **2**. Together with the mass spectrometric analysis mentioned above, we were able to deduce that the only difference between **2** and **1** was the chlorination of the 2,3-DHB unit at C-5, resulting in 4-chloro-2,3-dihydroxybenzoate (CDB) moiety. The molecular mass of **3** is increased by CH_2 relative to **2**, along with the changes of chemical shifts and splitting pattern of methyl groups, suggesting **2** and **3** differed in the fatty acyl groups. Detailed analysis of the NMR data showed that **3** contains an 8-methyldecanoate moiety attached to the δ-*N*-haOrn5 instead of the 8-methylnonanoate unit in **1** and **2** (Fig. S8). Thus, the planar structures of nobachelins A-C (**1**–**3**) were characterized (Fig. 2). To the best of our knowledge, CDB is rarely found in natural products, and only a few halogenated siderophores have been reported, such as chlorocatechelins A-B from *Streptomyces* sp. and teredinibactins from *Teredinibacter turnerae* [29,30].

In addition, several minor products with different acyl groups attached to the δ-*N*-haOrn5 were detected through LC-MS analysis (Fig. S9). Although we did not obtain sufficient amounts of these minor products for NMR analysis, their structures were deduced based on the MS/MS fragmentation data (Fig. S10).

The absolute configuration of the amino acids was determined using Marfey's method. The nobachelin B acid hydrolysate was derivatized using FDLA. The resulting reaction mixture was subjected to LC-MS analysis and compared with commercially available amino acid standards, which revealed the presence of L-Orn, L-Ser, and D-Ser in nobachelin B (Fig. S5). Considering the presence of one epimerization (E) domain in module 4 of NchH, the stereochemical configuration of the D-Ser in nobachelins was further corroborated.

Table 1
NMR spectroscopic data of nobachelin A-C (**1**–**3**) (DMSO-d_6).

no.	1		2		3	
	δ_H (*J* in Hz)	δ_C	δ_H (*J* in Hz)	δ_C	δ_H (*J* in Hz)	δ_C
DHB/CDB						
1		169.8		169.8		169.7
2		115.2		113.3		113.2
3		149.3		150.9		150.8
4		146.2		142.5		142.6
5	6.92 (1H, dd, 7.9, 1.4)	118.9		123.8		123.6
6	6.69 (1H, t, 7.9)	118.1	6.89 (1H, d, 8.8)	118.8	6.88 (1H, brs)	118.7
7	7.31 (1H, dd, 7.9, 1.4)	117.7	7.37 (1H, d, 8.8)	117.8	7.34 (1H, d, 8.8)	117.8
Gly1						
1		168.9		168.7		168.7
2	3.94 (1H, d, 5.8)	42.3	3.95 (1H, d, 5.8)	42.2	3.94 (1H, d, 5.4)	42.2
NH	9.08 (1H, t, 5.8)		9.22 (1H, t, 5.8)		9.23 (1H, brs)	
Gly2						
1		169.0		168.9		168.9
2	3.81 (1H, d, 5.6)	42.1	3.81 (1H, d, 5.8)	42.1	3.81 (1H, d, 5.7)	42.0
NH	8.31 (1H, t, 5.6)		8.33 (1H, t, 5.8)		8.31 (1H, t, 5.6)	
Ser3						
1		170.1		170.1		170.1
2	4.32 (1H, dd, 13.0, 5.5)	55.2	4.32 (1H, dd, 13.0, 5.5)	55.3	4.32 (1H, dd, 13.0, 5.6)	55.2
3	3.58 (2H, m[a])	61.7	3.58 (2H, m[a])	61.7	3.58 (2H, m[a])	61.7
NH	8.06 (1H, d, 7.4)		8.06 (1H, d, 7.5)		8.05 (1H, d, 7.5)	
Ser4						
1		169.7		169.7		169.6
2	4.28 (1H, m[a])	55.4	4.27 (1H, m[a])	55.4	4.28 (1H, m[a])	55.3
3	3.58 (2H, m[a])	61.7	3.58 (2H, m[a])	61.6	3.58 (2H, m[a])	61.6
NH	7.97 (1H, d, 7.8)		7.96 (1H, d, 7.5)		7.94 (1H, d, 7.8)	
haOrn5						
1		171.2		171.2		171.2
2	4.25 (1H, m[a])	52.3	4.25 (1H, m[a])	52.3	4.26 (1H, m[a])	52.2
3	1.68 (1H, m) 1.48 (1H, m)	29.4	1.68 (1H, m) 1.48 (1H, m)	29.3	1.68 (1H, m) 1.48 (1H, m)	29.3
4	1.56 (1H, m) 1.50 (1H, m)	22.9	1.56 (1H, m) 1.50 (1H, m)	22.8	1.56 (1H, m) 1.51 (1H, m)	22.8
5	3.50 (1H, m) 3.40 (1H, m)	46.8	3.50 (1H, m) 3.40 (1H, m)	46.8	3.50 (1H, m) 3.40 (1H, m)	46.8
NH	7.95 (1H, d, 8.5)		7.93 (1H, d, 8.3)		7.92 (1H, d, 8.3)	
1′		173.0		172.9		172.9
2′	2.32 (2H, t, 7.3)	31.8	2.32 (2H, t, 7.6)	31.7	2.32 (2H, t, 7.3)	31.7
3′	1.46 (2H, m)	24.3	1.45 (2H, m)	24.2	1.46 (2H, m)	24.2
4′	1.24 (2H, m)	29.0	1.24 (2H, m)	28.9	1.24 (2H, m)	28.9
5′	1.24 (2H, m)	29.3	1.23 (2H, m)	29.2	1.24 (2H, m)	29.3
6′	1.23 (2H, m)	26.8	1.23 (2H, m)	26.7	1.25 (2H, m)	26.4

(*continued on next page*)

Table 1 (*continued*)

no.	1		2		3	
7′	1.13 (2H, m)	38.5	1.13 (2H, m)	38.5	1.26 (1H, m) 1.05 (1H, m)	36.0
8′	1.48 (1H, m)	27.5	1.48 (1H, m)	27.4	1.28 (1H, m)	33.7
9′	0.84 (3H, d, 6.6)	22.6	0.84 (3H, d, 6.6)	22.6	1.29 (1H, m) 1.09 (1H, m)	28.9
10′	0.84 (3H, d, 6.6)	22.6	0.84 (3H, d, 6.6)	22.6	0.82 (3H, t, 7.3)	19.1
11′					0.81 (3H, d, 6.4)	11.2
chOrn6						
1		164.7		164.7		164.7
2	4.29 (1H, m[a])	49.5	4.29 (1H, m[a])	49.5	4.30 (1H, m[a])	49.5
3	1.87 (1H, m) 1.65 (1H, m)	27.6	1.87 (1H, m) 1.65 (1H, m)	27.5	1.88 (1H, m) 1.64 (1H, m)	27.5
4	1.89 (1H, m) 1.84 (1H, m)	20.4	1.90 (1H, m) 1.85 (1H, m)	20.3	1.90 (1H, m) 1.85 (1H, m)	20.3
5	3.45 (1H, m)	51.3	3.46 (1H, m)	51.2	3.45 (1H, m)	51.2
NH	8.06 (1H, d, 8.5)		8.04 (1H, d, 8.6)		8.03 (1H, d, 7.5)	

[a] signal overlapped.

3.4. The biosynthesis proposal of nobachelins

In-silico analysis of the *nch* BGC and characterization of nobachelins allowed us to propose a biosynthesis pathway for the catecholate-peptide siderophores in *N. baichengensis* DSM 44845 (Fig. 3). The 2,3-DHB building block, synthesized from chorismate (by NchA, NchB, NchD), is activated by the stand-alone A domain protein, NchC and loaded onto the free-standing aryl carrier protein NchF. The resulting 2,3-DHB-*S*-NchF species serves as the starter unit for the N-terminal C domain of the NRPS NchG to initiate the peptidyl chain elongation. The peptide backbone is synthesized in a textbook colinear fashion via another five rounds of condensation by NchG and NchH to incorporate respective amino acid building blocks [31]. The ornithine *N*-monooxygenase NchE catalyzes the formation of the nonproteogenic amino acid hOrn [28,32]. The thioesterase (TE) domain in NchH releases the final product via an intramolecular nucleophilic substitution reaction [33]. NchJ showed 38.4% identity to Rv1347c, the *N*-acyl transferase responsible for transferring long-chain acyl moieties onto the mycobactin scaffold [34,35], suggesting its *N*-acylation function in the biosynthesis of nobachelins. In addition, the observation of nobachelin congeners with different acyl modifications implied substrate promiscuity of NchJ in the acylation step.

Intriguingly, the chlorination of the 2,3-DHB unit remains elusive because the *nch* cluster lacks halogenase genes. Comparative analysis of the *nch* cluster from different microorganisms revealed further insights, as we performed genome mining using the stand-alone A domain protein (NchC) as the bait, identifying highly homologous gene clusters in the genomes of various strains from the family *Nocardiopsidaceae* (Fig. S11). One gene encoding a putative tryptophan halogenase was found within the three *nch*-like clusters from the genomes of *Spinactinospora*

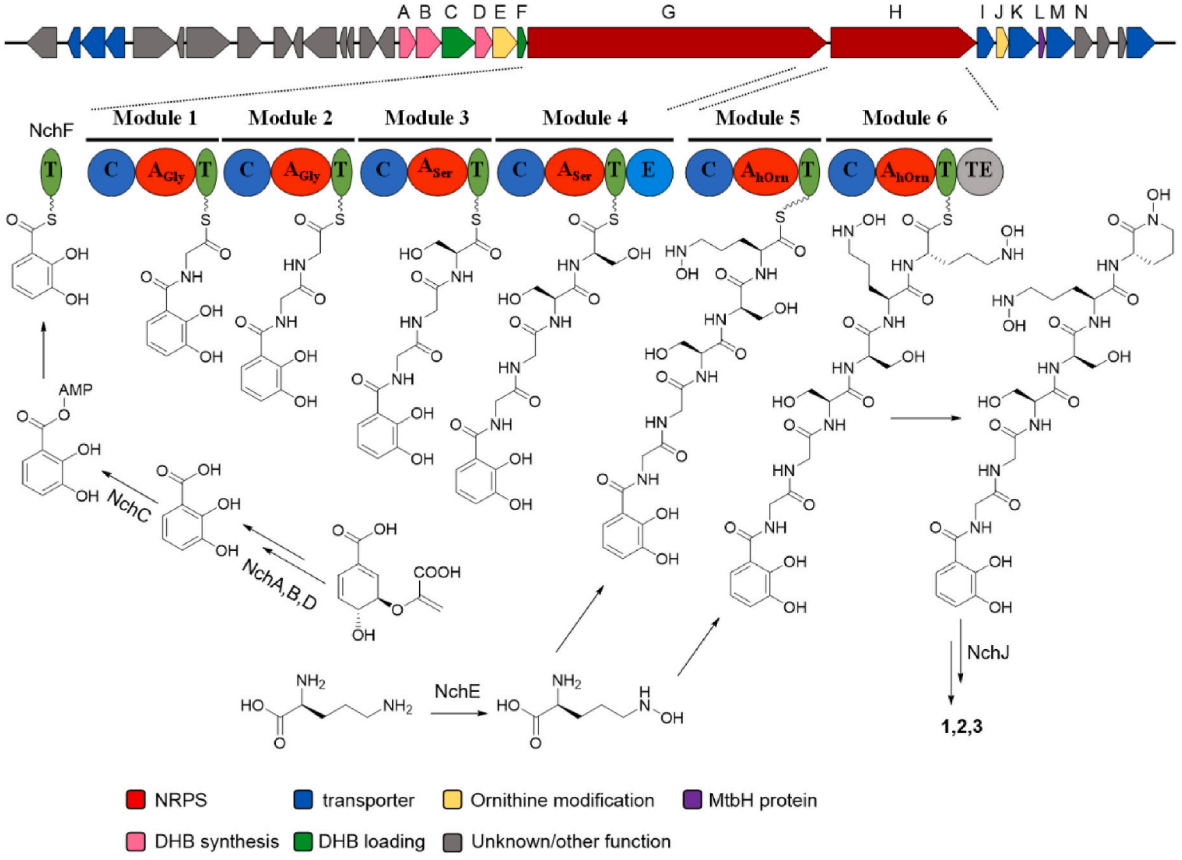

Fig. 3. Proposed biosynthesis pathway for the catecholate-peptide siderophore nobachelin in *Nocardiopsis baichengensis* DSM 44845. The 2,3-DHB was synthesized by NchABD, adenylated by NchD, and then transferred to NchF. The hexapeptide chain, synthesized by NchG and NchH, follows an orthodox colinear extension model. The acylation of Orn was catalyzed by the acyltransferase NchJ.

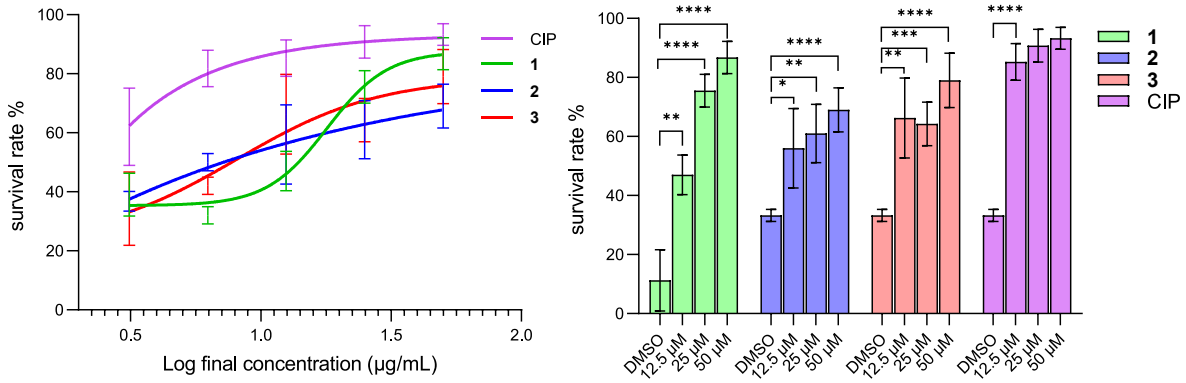

Fig. 4. Nobachelins rescue *C. elegans* from *P. aeruginosa* infection in a liquid killing assay. Ciprofloxacin (CIP) and DMSO were positive and negative controls, respectively. Four biological replicates were performed. Error bars represent SD. *p < 0.05, **p < 0.01, ***p < 0.001, ****p < 0.0001 (Student's *t*-test).

alkalitolerans [36], *Streptomonospora litoralis* [37] and *Streptomonospora salina* [38], respectively (Fig. S11, Table S5). Although absent in the *nch* cluster, a homologous gene encoding a putative tryptophan halogenase was located within another gene cluster of the strain *N. baichengensis* DSM 44845, suggesting the possible cross-talk effect for the formation of chlorinated nobachelins. Indeed, the utilization of distantly located enzymes is not an unusual phenomenon in siderophore biosynthesis [39–41]. Furthermore, HHpred analysis [42] of this halogenase revealed that it is homologous to a FAD-dependent halogenase, CndH, which introduces a chlorine atom to the tyrosyl moiety of the chondrochloren precursor [43,44]. Although we were able to detect both chlorinated and nonchlorinated nobachelins, it is difficult to determine the exact timing of chlorination during the nobachelin biosynthesis since tryptophan halogenases have been reported to chlorinate either the precursors [45,46] or the released compounds [47]. It is noteworthy that the stand-alone A domain in amychelin biosynthesis has been reported to accept both the chlorinated and nonchlorinated salicylate [14], which sheds light on the possibility of direct decoration of 2,3-DHB as the initial precursor.

3.5. Bioactivity assays

We investigated the anti-pathogenicity activity of isolated nobachelins using the *C. elegans-P. aeruginosa* liquid killing assay as reported [23]. The results showed a *C. elegans* rescuing effect of nobachelin A (**1**) and C (**3**) with EC_{50} values of 18.0 μg/mL and 8.5 μg/mL, respectively. Nobachelin B (**2**) also exhibited a positive effect, but its EC_{50} value was not determined (Fig. 4, Fig. S12). Moreover, **1**–**3** did neither exhibit cytotoxicity nor a direct antimicrobial activity against a panel of tested cell lines and bacterial and fungal strains (Table S6). These results provide additional support for the significant role of siderophores as potential anti-infectives that target host-pathogen interaction, as proposed previously [14].

4. Conclusions

Here, we employed a genome-guided and mass spectrometry-assisted strategy to identify a new group of siderophores, nobachelins, from *N. baichengensis* DSM 44845. Subsequent purification and structure elucidation revealed that nobachelins B–C feature a rare 4-chloro-2,3-dihydroxybenzoate moiety. Interestingly, while halogenase genes can be located within several *nch*-like clusters, a homologous gene was only found distant from the *nch* cluster in the genome of *N. baichengensis* DSM 44845. The functional interactions among BGCs located at distant locations are often observed, and such crosstalk might be essential for producing authentic products. However, bioinformatic analysis may not always accurately capture this interplay, highlighting the need for a holistic approach to natural product research.

Although no direct antimicrobial activity was observed from *in vitro* assays, nobachelins A-C (**1**–**3**) significantly improved the survival rate of *C. elegans* infected by *P. aeruginosa* PA14, suggesting some anti-virulence potential of nobachelins. This finding aligns with the previous report [14], corroborating the potential of siderophores in anti-infective discovery. It was also demonstrated that the iron-chelating ability of siderophores is not the sole determinant contributing to the *C. elegans*-protecting activity in the pathogenesis assay, as the Fe-chelated chloroamychelin is inactive while Fe-chelated fluoroamychelin I still exhibited activity [14]. Additionally, the Fe-free fluoroamychelin I showed better activity than that of chlorinated derivatives. Although the intricate mode of action behind these compounds remains obscure, our study paved the way for the optimization of nobachelins for the development of new treatments for *P. aeruginosa* infections.

CRediT authorship contribution statement

Haowen Zhao: Formal analysis, interpretation, paper writing. **Yuhao Ren:** Compound isolation, Formal analysis, interpretation. **Feng Xie:** Conceptualization, microbiology experiments, Formal analysis, interpretation, paper writing. **Huanqin Dai:** Bioactivity test. **Hongwei Liu:** Bioactivity test. **Chengzhang Fu:** Formal analysis, interpretation, paper writing. **Rolf Müller:** Conceptualization, Supervision, paper writing.

Declaration of competing interest

Rolf Müller is an editorial board member for *Synthetic and Systems Biotechnology* and was not involved in the editorial review or the decision to publish this article. All authors declare that there are no competing interests.

The authors declare that they have no known competing financial interests or personal relationships that could have appeared to influence the work reported in this paper.

Acknowledgements

Rolf Müller and Chengzhang Fu acknowledge support from the Helmholtz International Lab (InterLabs0007). Yuhao Ren acknowledges the support from the International Postdoctoral Exchange Fellowship Program (ZD202125) between Helmholtz Association, Germany and the Office of China Postdoc Council (OCPC), China. The authors appreciate the cell-based bioactivity test by Viktoria George and Alexandra Amann.

Appendix A. Supplementary data

Supplementary data to this article can be found online at https://doi.org/10.1016/j.synbio.2023.09.007.

References

[1] Genilloud O. Actinomycetes: still a source of novel antibiotics. Nat Prod Rep 2017; 34:1203–32. https://doi.org/10.1039/C7NP00026J.

[2] Atanasov AG, Zotchev SB, Dirsch VM. International natural product sciences T, supuran CT, natural products in drug discovery: advances and opportunities. Nat Rev Drug Discov 2021;20:200–16. https://doi.org/10.1038/s41573-020-00114-z.

[3] Medema MH, Fischbach MA. Computational approaches to natural product discovery. Nat Chem Biol 2015;11:639–48. https://doi.org/10.1038/nchembio.1884.

[4] Krug D, Müller R. Secondary metabolomics: the impact of mass spectrometry-based approaches on the discovery and characterization of microbial natural products. Nat Prod Rep 2014;31:768–83. https://doi.org/10.1039/C3NP70127A.

[5] Blin K, Shaw S, Kloosterman AM, Charlop-Powers Z, van Wezel GP, Medema MH, et al. antiSMASH 6.0: improving cluster detection and comparison capabilities. Nucleic Acids Res 2021;49:W29–35. https://doi.org/10.1093/nar/gkab335.

[6] Covington BC, McLean JA, Bachmann BO. Comparative mass spectrometry-based metabolomics strategies for the investigation of microbial secondary metabolites. Nat Prod Rep 2017;34:6–24. https://doi.org/10.1039/C6NP00048G.

[7] Wang M, Carver JJ, Phelan VV, Sanchez LM, Garg N, Peng Y, et al. Sharing and community curation of mass spectrometry data with global natural products social molecular networking. Nat Biotechnol 2016;34:828–37. https://doi.org/10.1038/nbt.3597.

[8] Khan A, Singh P, Srivastava A. Synthesis, nature and utility of universal iron chelator – siderophore: a review. Microbiol Res 2018;212–213:103–11. https://doi.org/10.1016/j.micres.2017.10.012.

[9] Kurth C, Kage H, Nett M. Siderophores as molecular tools in medical and environmental applications. Org Biomol Chem 2016;14:8212–27. https://doi.org/10.1039/C6OB01400C.

[10] Elalfy MS, Adly AM, Wali Y, Tony S, Samir A, Elhenawy YI. Efficacy and safety of a novel combination of two oral chelators deferasirox/deferiprone over deferoxamine/deferiprone in severely iron overloaded young beta thalassemia major patients. Eur J Haematol 2015;95:411–20. https://doi.org/10.1111/ejh.12507.

[11] Sato T, Yamawaki K. Cefiderocol: discovery, chemistry, and *in vivo* profiles of a novel siderophore cephalosporin. Clin Infect Dis 2019;69:S538–43. https://doi.org/10.1093/cid/ciz826.

[12] Petrik M, Zhai C, Haas H, Decristoforo C. Siderophores for molecular imaging applications. Clin Transl Imaging 2017;5:15–27. https://doi.org/10.1007/s40336-016-0211-x.

[13] Kunos CA, Ivy SP. Triapine radiochemotherapy in advanced stage cervical cancer. Front Oncol 2018;8:149. https://doi.org/10.3389/fonc.2018.00149.

[14] Xie F, Dai S, Zhao Y, Huang P, Yu S, Ren B, et al. Generation of fluorinated amychelin siderophores against *Pseudomonas aeruginosa* infections by a combination of genome mining and mutasynthesis. Cell Chem Biol 2020;27:1532–43. https://doi.org/10.1016/j.chembiol.2020.10.009.

[15] Hider RC, Kong X. Chemistry and biology of siderophores. Nat Prod Rep 2010;27:637–57. https://doi.org/10.1039/B906679A.

[16] Hofmann M, Retamal-Morales G, Tischler D. Metal binding ability of microbial natural metal chelators and potential applications. Nat Prod Rep 2020;37:1262–83. https://doi.org/10.1039/c9np00058e.

[17] Barry SM, Challis GL. Recent advances in siderophore biosynthesis. Curr Opin Chem Biol 2009;13:205–15. https://doi.org/10.1016/j.cbpa.2009.03.008.

[18] Bruns H, Crüsemann M, Letzel A-C, Alanjary M, Jo McInerney, Jensen PR, et al. Function-related replacement of bacterial siderophore pathways. ISME J 2018;12:320–9. https://doi.org/10.1038/ismej.2017.137.

[19] Timofeeva AM, Galyamova MR, Sedykh SE. Bacterial siderophores: classification, biosynthesis, perspectives of use in agriculture. Plants 2022;11:3065. https://doi.org/10.3390/plants11223065.

[20] Bennur T, Ravi Kumar A, Zinjarde SS, Javdekar V. *Nocardiopsis* species: a potential source of bioactive compounds. J Appl Microbiol 2016;120:1–16. https://doi.org/10.1111/jam.12950.

[21] Ibrahim AH, Desoukey SY, Fouad MA, Kamel MS, Gulder TAM, Abdelmohsen UR. Natural product potential of the genus *Nocardiopsis*. Mar Drugs 2018;16:147. https://doi.org/10.3390/md16050147.

[22] Shi T, Wang YF, Wang H, Wang B. Genus *Nocardiopsis*: a prolific producer of natural products. Mar Drugs 2022;20:374. https://doi.org/10.3390/md20060374.

[23] Kirienko NV, Cezairliyan BO, Ausubel FM, Powell JR. *Pseudomonas aeruginosa* PA14 pathogenesis in *Caenorhabditis elegans*. In: Filloux A, Ramos J-L, editors. Pseudomonas methods protoc. New York, NY: Springer New York; 2014. p. 653–69. https://doi.org/10.1007/978-1-4939-0473-0_50.

[24] Zhou YM, Shao L, Li JA, Han LZ, Cai WJ, Zhu CB, et al. An efficient and novel screening model for assessing the bioactivity of extracts against multidrug-resistant *Pseudomonas aeruginosa* using *Caenorhabditis elegans*. Biosci, Biotechnol, Biochem 2011;75:1746–51. https://doi.org/10.1271/bbb.110290.

[25] Kirienko NV, Kirienko DR, Larkins-Ford J, Wählby C, Ruvkun G, Ausubel FM. *Pseudomonas aeruginosa* disrupts *Caenorhabditis elegans* iron homeostasis, causing a hypoxic response and death. Cell Host Microbe 2013;13:406–16. https://doi.org/10.1016/j.chom.2013.03.003.

[26] Miethke M, Marahiel MA. Siderophore-based iron acquisition and pathogen control. Microbiol Mol Biol Rev 2007;71:413–51. https://doi.org/10.1128/MMBR.00012-07.

[27] Vetting MW, Carvalho LPSd, Yu M, Hegde SS, Magnet S, Roderick SL, et al. Structure and functions of the GNAT superfamily of acetyltransferases. Arch Biochem Biophys 2005;433:212–26. https://doi.org/10.1016/j.abb.2004.09.003.

[28] Ge L, Seah SYK. Heterologous expression, purification, and characterization of an L-Ornithine N^5-hydroxylase involved in pyoverdine siderophore biosynthesis in *Pseudomonas aeruginosa*. J Bacteriol 2006;188:7205–10. https://doi.org/10.1128/JB.00949-06.

[29] Miller BW, Schmidt EW, Concepcion GP, Haygood MG. Halogenated metal-binding compounds from shipworm symbionts. J Nat Prod 2022;85:479–84. https://doi.org/10.1021/acs.jnatprod.1c01049.

[30] Kishimoto S, Nishimura S, Hattori A, Tsujimoto M, Hatano M, Igarashi M, et al. Chlorocatechelins A and B from *Streptomyces* sp.: new siderophores containing chlorinated catecholate groups and an acylguanidine structure. Org Lett 2014;16:6108–11. https://doi.org/10.1021/ol502964s.

[31] Finking R, Marahiel MA. Biosynthesis of nonribosomal peptides. Annu Rev Microbiol 2004;58:453–88. https://doi.org/10.1146/annurev.micro.58.030603.123615.

[32] Pohlmann V, Marahiel MA. δ-Amino group hydroxylation of L-ornithine during coelichelin biosynthesis. Org Biomol Chem 2008;6:1843–8. https://doi.org/10.1039/B801016A.

[33] Bosello M, Zeyadi M, Kraas FI, Linne U, Xie X, Marahiel MA. Structural characterization of the heterobactin siderophores from *Rhodococcus erythropolis* PR4 and elucidation of their biosynthetic machinery. J Nat Prod 2013;76:2282–90. https://doi.org/10.1021/np4006579.

[34] Krithika R, Marathe U, Saxena P, Ansari MZ, Mohanty D, Gokhale RS. A genetic locus required for iron acquisition in *Mycobacterium tuberculosis*. Proc Natl Acad Sci U S A 2006;103:2069–74. https://doi.org/10.1073/pnas.0507924103.

[35] Card GL, Peterson NA, Smith CA, Rupp B, Schick BM, Baker EN. The crystal structure of Rv1347c, a putative antibiotic resistance protein from *Mycobacterium tuberculosis*, reveals a GCN5-related fold and suggests an alternative function in siderophore biosynthesis. J Biol Chem 2005;280:13978–86. https://doi.org/10.1074/jbc.M413904200.

[36] Chang XB, Liu WZ, Zhang XH. *Spinactinospora alkalitolerans* gen. nov., sp. nov., an actinomycete isolated from marine sediment. Int J Syst Evol Microbiol 2011;61:2805–10. https://doi.org/10.1099/ijs.0.027383-0.

[37] Khodamoradi S, Hahnke RL, Mast Y, Schumann P, Kämpfer P, Steinert M, et al. *Streptomonospora litoralis* sp. nov., a halophilic thiopeptides producer isolated from sand collected at Cuxhaven beach. Antonie Leeuwenhoek 2021;114:1483–96. https://doi.org/10.1007/s10482-021-01609-4.

[38] Li WJ, Xu P, Zhang LP, Tang SK, Cui XL, Mao PH, et al. *Streptomonospora alba* sp. nov., a novel halophilic actinomycete, and emended description of the genus *Streptomonospora Cui* et al. Int J Syst Evol Microbiol 2001;2003(53):1421–5. https://doi.org/10.1099/ijs.0.02543-0.

[39] Chen J, Frediansyah A, Männle D, Straetener J, Brötz-Oesterhelt H, Ziemert N, et al. New nocobactin derivatives with antimuscarinic activity, terpenibactins A–C, revealed by genome mining of *Nocardia terpenica* IFM 0406. Chembiochem 2020;21:2205–13. https://doi.org/10.1002/cbic.202000062.

[40] Hoshino Y, Chiba K, Ishino K, Fukai T, Igarashi Y, Yazawa K, et al. Identification of nocobactin NA biosynthetic gene clusters in *Nocardia farcinica*. J Bacteriol 2011;193:441–8. https://doi.org/10.1128/jb.00897-10.

[41] Seyedsayamdost MR, Traxler MF, Zheng SL, Kolter R, Clardy J. Structure and biosynthesis of amychelin, an unusual mixed-ligand siderophore from *Amycolatopsis* sp. AA4. J Am Chem Soc 2011;133:11434–7. https://doi.org/10.1021/ja203577e.

[42] Zimmermann L, Stephens A, Nam S-Z, Rau D, Kübler J, Lozajic M, et al. A completely reimplemented MPI bioinformatics toolkit with a new HHpred server at its core. J Mol Biol 2018;430:2237–43. https://doi.org/10.1016/j.jmb.2017.12.007.

[43] Rachid S, Scharfe M, Blöcker H, Weissman KJ, Müller R. Unusual chemistry in the biosynthesis of the antibiotic chondrochlorens. Chem Biol 2009;16:70–81. https://doi.org/10.1016/j.chembiol.2008.11.005.

[44] Buedenbender S, Rachid S, Müller R, Schulz GE. Structure and action of the myxobacterial chondrochloren halogenase CndH: a new variant of FAD-dependent halogenases. J Mol Biol 2009;385:520–30. https://doi.org/10.1016/j.jmb.2008.10.057.

[45] Lin S, Van Lanen SG, Shen B. Regiospecific chlorination of (*S*)-β-tyrosyl-*S*-carrier protein catalyzed by SgcC3 in the biosynthesis of the enediyne antitumor antibiotic C-1027. J Am Chem Soc 2007;129:12432–8. https://doi.org/10.1021/ja072311g.

[46] Payne JT, Andorfer MC, Lewis JC. Regioselective arene halogenation using the FAD-dependent halogenase RebH. Angew Chem Int Ed 2013;52:5271–4. https://doi.org/10.1002/anie.201300762.

[47] Chankhamjon P, Boettger-Schmidt D, Scherlach K, Urbansky B, Lackner G, Kalb D, et al. Biosynthesis of the halogenated mycotoxin aspirochlorine in koji mold involves a cryptic amino acid conversion. Angew Chem Int Ed 2014;53:13409–13. https://doi.org/10.1002/anie.201407624.